Earthquake Geotechnical Engineering for Protection and Development of Environment and Constructions – Silvestri & Moraci (Eds)
© 2019 Associazione Geotecnica Italiana, Rome, Italy, ISBN 978-0-367-14328-2

Identification of surface waves generated in a sedimentary basin in Japan

K.C. Meza-Fajardo & H. Aochi
BRGM, Orleans, France

A.S. Papageorgiou
University of Patras, Greece

ABSTRACT: Recent events have allowed the observation of the effects of long-period motions on large-scale structures in Japan, and their devastating consequences. In this work we investigate the generation of surface waves in the basin of Nagoya (Nobi plain) in Japan, from seismograms of the K-net network, including recordings of the Mw 9.0 2011 Tohoku earthquake. The surface waves are identified by their polarization characteristics when the seismogram is represented in the time-frequency space via the S-Transform. We adopt the "Normalized Inner Product" (NIP) as criterion to quantify the polarization features of the different train waves, since the NIP can be considered as the time-frequency counterpart of correlation. We then apply filters based on the NIP to the S-Transform to isolate and extract the identified surface waves. With this procedure we provide the direction of propagation of the identified wavetrains, and then evaluate their mechanisms of generation.

1 INTRODUCTION

The importance of surface waves forming long-duration ground motion has been recognized by engineers and seismologists following the 1985 Michoacan earthquake in Mexico. Recent events in Japan, including the Mw 9.0 2011 Tohoku earthquake have also exposed the effects of long-period ground motions on large-scale structures (e.g., Çelebi et al., 2014; Koketsu et al., 2005). The Nagoya basin (also called Nobi plain) in Japan is a sediment filled valley with a complex structure and a superficial area of about 1300 square kilometers. The city of Nagoya, being the fourth-most-populous urban area in Japan with more than 2 million people, is located on the basin. The city has suffered extensive damage during large earthquakes in the past, being the 1891 Nobi earthquake the most dramatic example.

Many studies in Japan focusing on the Kanto and Osaka basin (e.g. Furumura & Hayakawa, 2007; Kato et al., 1993) have observed that the late-arriving surface waves are generated at the edges of sedimentary basins. In this work we study surface waves generated at the sedimentary basin of Nagoya from analysis of strong ground motion recorded by the K-net seismographic network during different seismic events. The basin characteristics are retrieved from the 3D national deep structure model of the National Research Institute for Earth Science and Disaster Resilience (NIED). First, we extract surface waves from the recorded ground motions along with its direction of polarization at each station. In this process, we differentiate between the surface waves incoming into the basin and the surface waves generated at the basin. Our analysis indicates that the surface waves generated at the basin are of frequencies above 0.12 Hz. We then asses the relation between different parameters defining the extracted surface waves (amplitude, duration) and the basin depth.

2 DATA

The Nobi plain, located in the central part of Japan (Figure 1), is a deep, complex plain composed of Alluvial, Pleistocene and Tertiary strata. Long period ground motions between 3 and 6 seconds have been predicted in the basin from numerical simulations (Kawabe & Kamae, 2005) under large earthquakes. The area considered in this study is shown in Figure 1, as well as the epicentral location of the events. Besides different azimuthal directions (with respect to the basin), we analyzed the Chuetsu and Tohoku earthquakes as shown in Table 1.

Strong ground motion records from the K-net network were retrieved at rock outcrops sites and at sites within the basin. The spatial distribution of the stations considered in the study is shown in Figure 2, although not all stations recorded the events. On the other hand, the 3D depth structure of the basin was retrieved from the National Research Institute for Earth Science and Disaster Resilience (NIED) of Japan (http://www.j-shis.bosai.go.jp). Figure 3 shows the spatial variation of the bedrock depth corresponding the upper depth of a layer of Vs=2700m/s. We can observe that the basin has a complex 3D structure with sharp horizontal variation at the edges, and with maximum depth reaching 3 km. Furthermore the southern part of the basin is covered by sea water. The displacement waveforms were derived from the

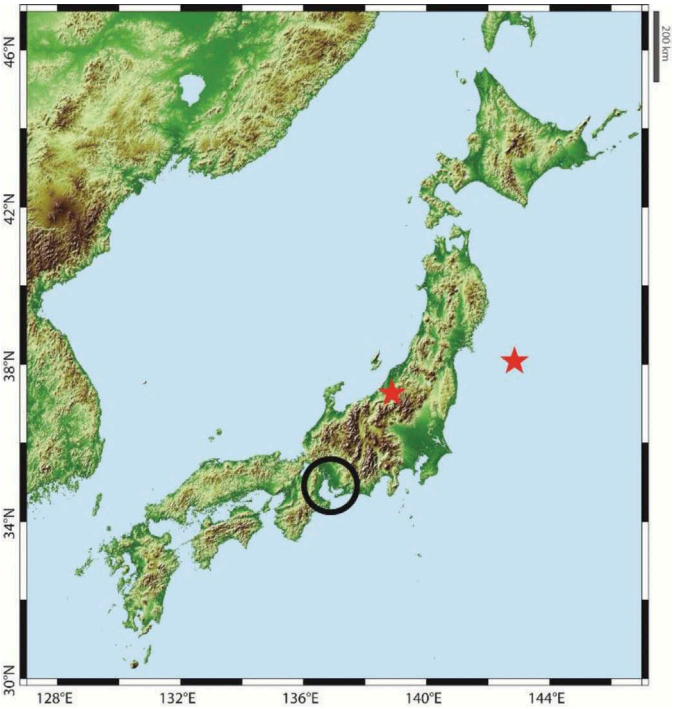

Figure 1. Location of Nagoya basin (indicated by the black circle) and epicentral location (red stars) of the events considered in this study.

Table 1. Earthquakes considered for surface wave analysis in Nobi plain (Nagoya basin). Earthquake informations are based on the catalogue of Japan Meteorological Agency. Time is local time (JST).

Name	Event time	Magnitude M_{JMA}	Latitude	Longitude	Depth (Km)	Note
Chuetsu	2004/10/23 17:56:00	6.8	37.291	138.867	13	Crustal reverse faulting
Tohoku	2011/03/11 14:46:00	9.0	38.103	142.86	24	subduction

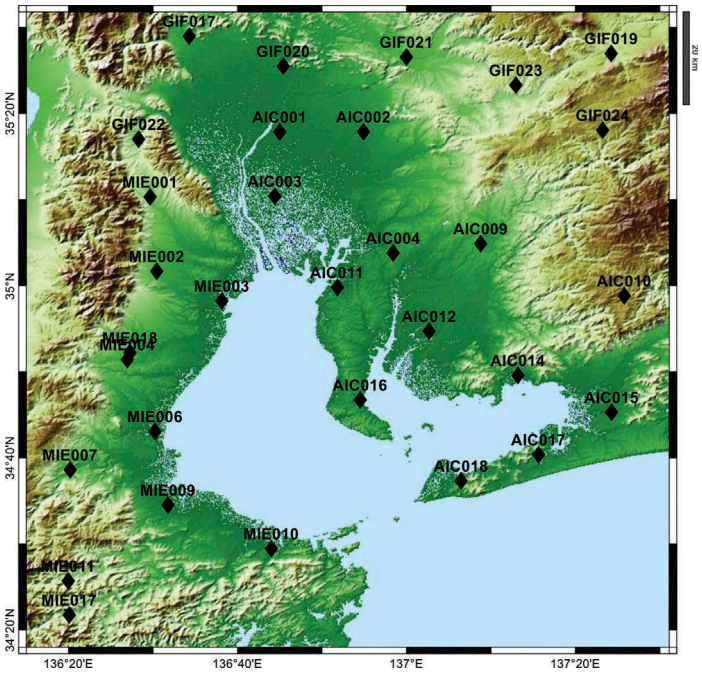

Figure 2. Location of K-net seismographic stations used in the study.

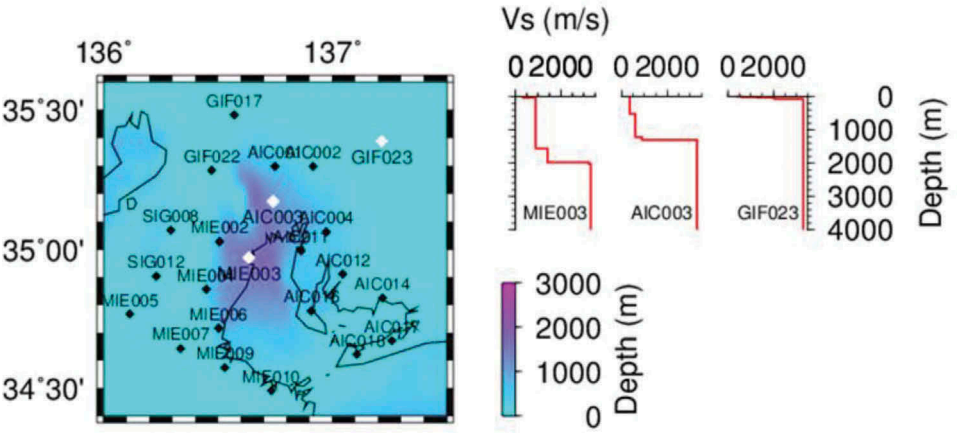

Figure 3. The upper depth of a layer of Vs=2700 m/s from the 3D deep structure model provided by NIED. The Vs profiles are also shown for the three stations MIE003, AIC003 and GIF023.

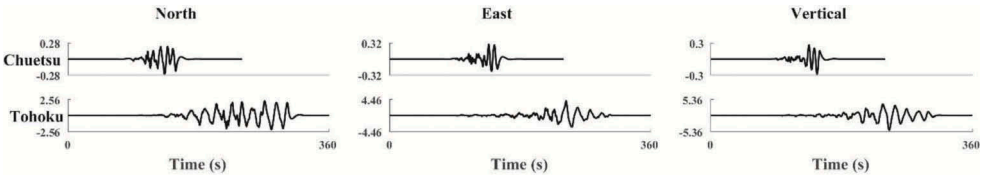

Figure 4. North, East and vertical components of displacement histories in cm at station GIF023 corresponding to events listed in Table 1.

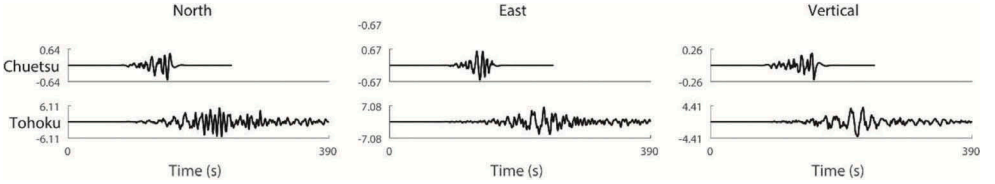

Figure 5. North, East and vertical components of displacement histories at station MIE003 corresponding to events listed in Table 1.

recorded acceleration histories, by band-pass filtering between 0.05 and 20 Hz, and then integrating in time twice. In Figures 4 and 5 we show the three components of the obtained displacement histories for stations GIF023 and MIE003, respectively, corresponding to the two events listed in Table 1. For station GIF023, which can be considered on hard rock (see Figure 2), we can observe the different amplitudes, frequency content and duration related to the two events. These differences can be also observed at station MIE003, however, we can observe longer amplification, changes in frequency content and duration when compared to station GIF023. As this station is in the deeper part of the basin (see Figure 2), we interpret the observed variations as the effects of basin-generated surface waves.

3 METHOD OF SURFACE WAVE ANALYSIS

In order to study surface waves in the Nobi plain we make use of a time-frequency method based on the Normalized Inner Product (NIP) to identify and extract the surface waves (Meza-Fajardo et al., 2015). The basic idea of the method is to separate the waves by representing their polarization characteristics in terms of orthogonal relations in the time-frequency domain. The inner product (NIP) is then naturally implemented to establish orthogonality. Each component of the seismogram is first resolved in the time-frequency domain by using the Stockwell Transform:

$$S(t,f) = \int_{-\infty}^{\infty} h(\tau)\frac{|f|}{\sqrt{2\pi}}\exp\left[-\frac{(t-\tau)^2 f^2}{2}\right]\exp(-2\pi i f\tau)d\tau \tag{1}$$

We denote the Stockwell transforms of the North, East and vertical components of the signal by $S_N(t,f)$, $S_E(t,f)$ and $S_V(t,f)$, respectively. Each of these discrete Stockwell transforms is a matrix defined in the discretized (t,f) space, and each element of the matrix is a complex number. Therefore, each Stockwell Transform may be expressed as follows:

$$S_c(t,f) = A_c(t,f)\exp[i\cdot\Phi_c(t,f)] \tag{2}$$

where $i=\sqrt{-1}$, $A_c(t,f)$ is the amplitude of $S_c(t,f)$, and $\Phi_c(t,f)$ is its phase. Then, the "normalized inner product" (NIP) between two Stockwell Transforms is defined as follows:

$$NIP(S_c\ , S_m) = \frac{\mathrm{Re}\{S_c(t,f)\}\mathrm{Re}\{S_m(t,f)\} + \mathrm{Im}\{S_c(t,f)\}\mathrm{Im}\{S_m(t,f)\}}{A_c(t,f)A_m(t,f)} \tag{3}$$

The inner product is a simple, well-known, mathematical relation used to identify orthogonality properties between two entities. It can be also considered as a surrogate of the time-domain "correlation". It turns out useful to identify Rayleigh waves since there is a $\pm(\pi/2)$ phase shift between its horizontal and vertical components. Then, it can be used to identify the direction of polarization of the horizontal component of the Rayleigh wave, because with the NIP we find the two orthogonal horizontal directions in which the correlation is minimum. Furthermore, if we perform a $\pm(\pi/2)$ shift in the vertical component S_V of a Rayleigh wave, then the resulting Transform $\hat{S}_V$ will be in phase with the horizontal component and

$NIP\left(S_H, \hat{S}_V\right) = 1$. Then, using the relation $NIP\left(S_H, \hat{S}_V\right)$ we can construct simple filters to retain only those regions in the time-frequency space in which the value of $NIP\left(S_H, \hat{S}_V\right)$ is close to 1 [say, $NIP\left(S_H, \hat{S}_V\right) \geq 0.8$] and setting the rest of the time-frequency space equal to zero. Details on the procedure to extract surface waves using the Stockwell Transform can be found in (Meza-Fajardo et al., 2015; Meza-Fajardo & Papageorgiou, 2016).

4 RESULTS

We start our analysis focusing on the recordings of the Tohoku earthquake. Because of its large size, this earthquake generated sufficient energy at very low frequencies. In Figure 6(a) and 6(b) we first show the extracted retrograde Rayleigh waves in a frequency band between 0.05 and 0.12 Hz. Figure 6(a) shows the location of the stations and the direction the Rayleigh

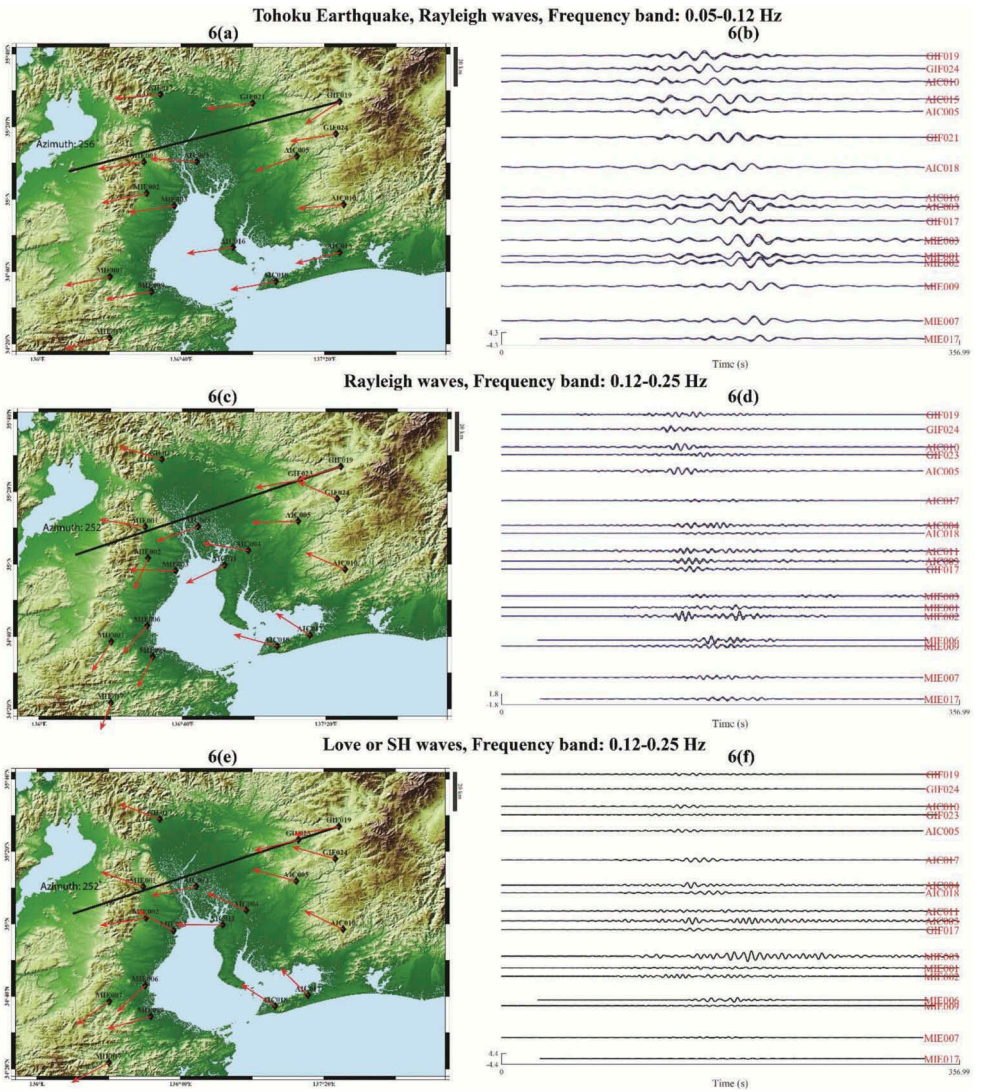

Figure 6. Surface waves extracted from recording of Tohoku Earthquake. The red arrows indicate the direction of polarization.

waves are polarized, which coincides with their direction of propagation. The black line illustrates the average direction of all stations shown. In Figure 6(b) we show the waveforms of the extracted Rayleigh waves. Both, the horizontal (in black), and the vertical component with a $\pi/2$ shift (in blue) are plotted to show they are well correlated and therefore, the extracted waves can be regarded as Rayleigh waves. We observe that the Rayleigh waves of Figures 6(a) and 6(b) do not change significantly their direction of propagation, nor their waveform as they travel through the basin.

Thus, these waves are not related to the basin, but are incoming waves generated by the interaction of the seismic energy with the crust's surface. On the other hand, the middle panels of Figures 6(c) and 6(d) show extracted retrograde Rayleigh waves in the frequency band between 0.12 and 0.25 Hz. We can also observe these Rayleigh waves are not generated at the basin, but nevertheless they interact with it. To the west-south of station MIE003 the direction of the extracted Rayleigh waves becomes southwest, indicating some of the energy is diffracted by the basin. Furthermore in Figures 6(e) and 6(f) we show linearly polarized waves, which can be regarded as SH or as Love waves, again in the frequency band between 0.12 and 0.25 Hz. It is important to note that the red arrows indicate their direction of polarization, which is not necessarily their direction of propagation. We can see that the energy in this form of (linearly polarized) waves is not significant outside the basin, but we find strong amplitudes and longer durations at the stations located on the deeper part of the basin, for example, stations MIE003 and AIC003. These results indicate that the frequencies affected by the basin (giving rise to basin effects) are those greater than 0.12 Hz.

In Figure 7 we show similar wavemaps of extracted retrograde Rayleigh and Love waves for the Chuetsu earthquake. In the analyses of this event, we consider only frequencies above 0.12 Hz. Once again, the results indicate that the extracted Rayleigh waves are not generated

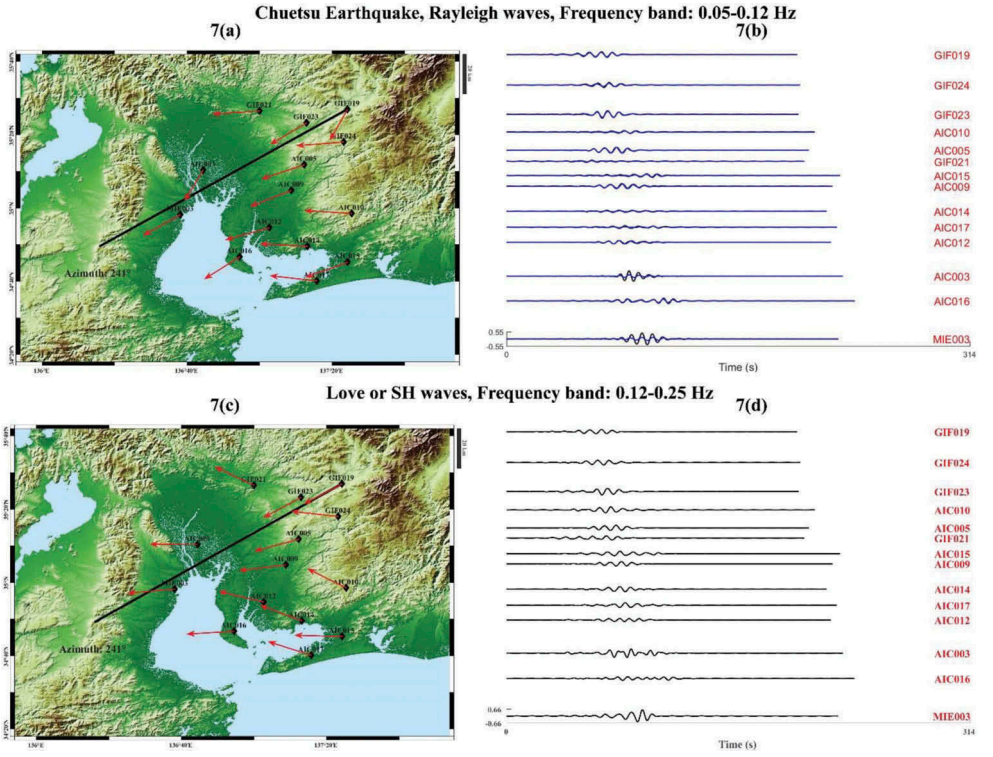

Figure 7. Surface waves extracted from recording of Chuetsu Earthquake. The red arrows indicate the direction of polarization.

at the basin as they are found at stations outside the basin as well. However, we can observe amplification of the horizontal component of the Rayleigh waves at the deeper stations of the basin (MIE003 and AIC003 for example). The remaining waves after extracting the Rayleigh waves, and that are linearly polarized (SH or Love waves), are shown in Figures 7(c) and 7(d). At the deeper parts of the basin these waves have different direction of polarization relative to the Rayleigh waves. Contrary to the case of the Tohoku earthquake, the waves extracted (in the range 0.12–0.25 Hz) from the Chuetsu recordings are not much affected by their propagation through the basin, probably because their frequencies fall into the lower end of the frequency band (close to 0.12 Hz).

CONCLUSIONS

We have identified and extracted surface waves propagating in the Nobi plain (basin of Nagoya), from seismograms of the strong-motion seismograph networks (K-net, Kik-net) of Japan. With our time-frequency technique we have estimated the direction of polarization and then extracted the waveforms of Rayleigh and Love waves. Considering several earthquakes with different magnitudes and location relative to the basin, our analyses indicated that Rayleigh waves are present in the seismograms, but they are not generated due to basin effects, nor they undergo significant amplification. However, incoming energy above 0.12 Hz gives rise to Love waves on the deeper parts of the basin, where important amplification and duration is observed. Our study suggests that the main effect that can be attributed to the basin structure is the elongated duration of the ground motion. Ground motion of long duration should then be an important consideration for the urban development in the Nagoya area, because of its impact on the non-linear response of structures, and the potential of soil liquefaction, especially for sites near the coast.

REFERENCES

Çelebi, M., Okawa, I., Kashima, T., Koyama, S., & Iiba, M. 2014. Response of a tall building far from the epicenter of the 11 March 2011 M9.0 Great East Japan earthquake and aftershocks. *The Structural Design of Tall and Special Buildings*, 421–439. https://doi.org/10.1002/tal.1047

Furumura, T., & Hayakawa, T. 2007. Anomalous propagation of long-period ground motions recorded in Tokyo during the 23 October 2004 Mw 6.6 Niigata-ken Chuetsu, Japan, earthquake. *Bulletin of the Seismological Society of America*, *97*(3), 863–880. https://doi.org/10.1785/0120060166

Kato, K., Aki, K., & Teng, T. 1993. 3-D simulations of surface wave propagation in the Kanto sedimentary basin, Japan–part 1: Application of the surface wave gaussian beam method. *Bulletin of the Seismological Society of America*, *83*(6), 1676–1699.

Kawabe, H., & Kamae, K. 2005. Long period ground motion prediction of linked Tonankai and Nankai subduction earthquakes using 3D finite difference method. San Francisco: American Geophysical Union, Fall Meeting 2005, abstract id. S21B–0213.

Koketsu, K., Hatayama, K., Furumura, T., Ikegami, Y., & Akiyama, S. 2005. Damaging long-period ground motions from the 2003 Mw 8.3 Tokachi-oki, Japan earthquake. *Seismological Research Letters*, *76*(1), 67–73. https://doi.org/10.1785/gssrl.76.1.67

Meza-Fajardo, K. C., & Papageorgiou, A. S. 2016. Estimation of rocking and torsion associated with surface waves extracted from recorded motions. *Soil Dynamics and Earthquake Engineering*, *80*. https://doi.org/10.1016/j.soildyn.2015.10.017

Meza-Fajardo, K. C., Papageorgiou, A. S., & Semblat, J.F. 2015. Identification and extraction of surface waves from three-component seismograms based on the normalized inner product. *Bulletin of the Seismological Society of America*, *105*(1). https://doi.org/10.1785/0120140012